https://doi.org/10.1093/brain/awad130 BRAIN 2023: 146; 4088–4104 | 4088

BRAIN
ORIGINAL ARTICLE

Abl kinase-mediated FUS Tyr526 phosphorylation alters nucleocytoplasmic FUS localization in FTLD-FUS

Helena Motaln,[1] Urša Čerček,[1,2] Alfred Yamoah,[3] Priyanka Tripathi,[3] Eleonora Aronica,[4] Anand Goswami[3,5,6,†] and Boris Rogelj[1,7,†]

[†]These authors contributed equally to this work.

Nuclear to cytoplasmic mislocalization and aggregation of multiple RNA-binding proteins (RBPs), including FUS, are the main neuropathological features of the majority of cases of amyotrophic lateral sclerosis (ALS) and frontotemporal lobular degeneration (FTLD). In ALS-FUS, these aggregates arise from disease-associated mutations in FUS, whereas in FTLD-FUS, the cytoplasmic inclusions do not contain mutant FUS, suggesting different molecular mechanisms of FUS pathogenesis in FTLD that remain to be investigated.

We have previously shown that phosphorylation of the C-terminal Tyr526 of FUS results in increased cytoplasmic retention of FUS due to impaired binding to the nuclear import receptor TNPO1. Inspired by the above notions, in the current study we developed a novel antibody against the C-terminally phosphorylated Tyr526 FUS ($FUS^{p\text{-}Y526}$) that is specifically capable of recognizing phosphorylated cytoplasmic FUS, which is poorly recognized by other commercially available FUS antibodies.

Using this $FUS^{p\text{-}Y526}$ antibody, we demonstrated a FUS phosphorylation-specific effect on the cytoplasmic distribution of soluble and insoluble $FUS^{p\text{-}Y526}$ in various cells and confirmed the involvement of the Src kinase family in Tyr526 FUS phosphorylation. In addition, we found that $FUS^{p\text{-}Y526}$ expression pattern correlates with active pSrc/pAbl kinases in specific brain regions of mice, indicating preferential involvement of cAbl in the cytoplasmic mislocalization of $FUS^{p\text{-}Y526}$ in cortical neurons. Finally, the pattern of immunoreactivity of active cAbl kinase and $FUS^{p\text{-}Y526}$ revealed altered cytoplasmic distribution of $FUS^{p\text{-}Y526}$ in cortical neurons of post-mortem frontal cortex tissue from FTLD patients compared with controls. The overlap of $FUS^{p\text{-}Y526}$ and FUS signals was found preferentially in small diffuse inclusions and was absent in mature aggregates, suggesting possible involvement of $FUS^{p\text{-}Y526}$ in the formation of early toxic FUS aggregates in the cytoplasm that are largely undetected by commercially available FUS antibodies.

Given the overlapping patterns of cAbl activity and $FUS^{p\text{-}Y526}$ distribution in cortical neurons, and cAbl induced sequestration of $FUS^{p\text{-}Y526}$ into G3BP1 positive granules in stressed cells, we propose that cAbl kinase is actively involved in mediating cytoplasmic mislocalization and promoting toxic aggregation of wild-type FUS in the brains of FTLD patients, as a novel putative underlying mechanism of FTLD-FUS pathophysiology and progression.

1 Department of Biotechnology, Jožef Stefan Institute, SI-1000 Ljubljana, Slovenia
2 Graduate School of Biomedicine, Faculty of Medicine, University of Ljubljana, SI-1000 Ljubljana, Slovenia
3 Institute of Neuropathology, RWTH Aachen University Medical School, 52074 Aachen, Germany
4 Amsterdam UMC location University of Amsterdam, Department of Neuropathology, Amsterdam Neuroscience, 1105 Amsterdam, The Netherlands

Received October 07, 2022. Revised March 02, 2023. Accepted March 28, 2023. Advance access publication April 18, 2023

5 Department of Neurology, Center for Motor Neuron Biology and Disease, Columbia University, New York, NY 10032, USA
6 Department of Neurology, Eleanor and Lou Gherig ALS Center, Columbia University, New York, NY 10032, USA
7 Faculty of Chemistry and Chemical Technology, University of Ljubljana, SI-1000 Ljubljana, Slovenia

Correspondence to: Boris Rogelj
Department of Biotechnology B3, Jozef Stefan Institute
Jamova 39, 1000 Ljubljana, Slovenia
E-mail: boris.rogelj@ijs.si

Keywords: FUS; phosphorylation; cytoplasmic aggregates; c-Src; c-Abl; FTLD

Introduction

Genomic approaches have linked mutations in genes of RNA-binding proteins (RBPs), to the pathogenesis of two overlapping but clinically heterogeneous neurodegenerative diseases, amyotrophic lateral sclerosis (ALS) and frontotemporal lobular degeneration (FTLD).[1-7] Mutations in the fused in sarcoma (*FUS*) gene are rare and found only in a small subset of ALS cases and do not appear to be a direct cause of FTLD.[8-11] Human FUS contains 526 amino acids and consists of the N-terminal low-complexity domain (LC) and a Gly-rich region, followed by an RNA-recognition motif (RRM), two Arg-Gly-Gly (RGG) repeat regions interrupted by a zinc finger motif, and a C-terminal PY-NLS (nuclear localization signal). Both RGG repeat regions and the C-terminal PY-NLS are critical for binding to transportin 1 (TNPO1), which is responsible for nuclear import of FUS under normal conditions. Although FUS-immunoreactive cytoplasmic inclusions are the major pathologic feature of familial (f)FUS-ALS cases,[9] FUS-positive, tau/TDP-43 negative inclusions are also present in FTLD cases (FTLD-FUS) but without genetic mutation in the *FUS* gene.[8,10] Elevated levels of full-length and fragmented FUS have also been detected in the cytoplasm of cerebral and spinal cord neurons[3,12] from ALS and FTLD patients and have been associated with impairment of RNA splicing, intra-axonal transport/translation, and synaptic function.[13,14]

The precise molecular mechanism of cytoplasmic FUS mislocalization and aggregation remains unclear, the presence of such cytoplasmic inclusions in both fALS-FUS and FTLD-FUS suggests that FUS mislocalization to the cytoplasm, together with its nuclear depletion, contributes to neurodegeneration through a combined loss-of-function and gain-of-toxicity mechanisms.[15-18] To understand FUS pathophysiology in detail, there is an urgent need to elucidate the signaling pathways affecting nucleocytoplasmic shuttling of FUS. In this regard, post-translational modifications of FUS have been proposed to contribute to FUS mislocalization, affect FUS phase separation (LLPS)[19-22] and toxicity, all of which are enhanced by chronic stress.[23] FUS LLPS is controlled by cation interactions between Tyr residues in the N-terminal LC-domain, and Arg residues and 526Tyr in the C-terminal domain.[9,24-26] Consistent with this, hypomethylation of Arg residues in FTLD-FUS promotes cytoplasmic FUS aggregation,[27,28] while phosphorylation of the N-terminal domain of FUS inhibits it.[29]

With this in mind, we aimed to decipher whether phosphorylation of 526Tyr FUS (FUS$^{p\text{-}Y526}$) has an effect on nucleocytoplasmic shuttling of FUS. We have previously shown that phosphorylation of 526Tyr FUS increases its cytoplasmic localization by inhibiting the binding of FUS to TNPO1.[2,24,30,31] To gain insight into the mechanism of Tyr526 FUS phosphorylation, we examined several stress-induced kinases associated with ALS-FTLD,[32] including the Ser/Thr kinases[10,12,13,29,33,34] and Tyr kinases of the non-receptor Src-family.[35-38] We have demonstrated that the Src, Fyn, and Abl kinases phosphorylate Tyr526 FUS.[26] These kinases are also known to be active in the brain.[39-41] Therefore we investigated the pattern of immunoreactivity of FUS$^{p\text{-}Y526}$ and active kinases (pSrc, pFyn, pAbl) in different neuronal-like/differentiated cell models, in primary neuronal mouse culture and in mouse brains, and finally compared it with frontal cortex tissue obtained from the brain of FTLD-FUS patients. The observed co-localizations and the varying degree of overlap in signal intensities between FUS$^{p\text{-}Y526}$ immunoreactivity and active kinases suggest kinase type-dependent subcellular localization of FUS$^{p\text{-}Y526}$ in HEK293T cells, differentiated NSC34 and SH-SY5Y cells, primary cortical neurons, and neurons in mouse brains. Interestingly, we observed significantly altered nucleocytoplasmic distribution of FUS$^{p\text{-}Y526}$ in the brains of FTLD-FUS patients compared with non-neurological normal control brain tissue. Although the majority of cortical neurons from FTLD-FUS patients showed diffuse cytoplasmic and moderate to strong nuclear localization of FUS$^{p\text{-}Y526}$, a significant percentage (10–20%) of cortical neurons also showed abnormal deposits of atypical granular, small globular cytoplasmic accumulation of FUS$^{p\text{-}Y526}$, as well as loss of nuclear immunoreactivity in many neurons. Such FUS$^{p\text{-}Y526}$-positive granular and small globular aggregates were morphologically distinct from typical gel-like large FUS aggregates and were rarely co-localized together. Consistent with the notion that FUS aggregation may proceed via stress-granule pathways, we observed that Abl kinase indeed promotes sequestration of FUS$^{p\text{-}Y526}$ into G3BP1-positive granules in stressed cells. Although future experiments are warranted to characterize such deposits of atypical smaller globular and granular FUS$^{p\text{-}Y526}$ accumulations and their precise role in FUS pathology, based on our observations, it can be assumed that they may be pathologically active and serve as precursors of larger toxic aggregates. Thus in summary, we propose that FUS$^{p\text{-}Y526}$ probably regulates stress-induced FUS aggregation along with the active involvement of Abl kinase and actively contributes to early FTLD-FUS pathology. The novel antibody platform we have developed is unique for screening the C-terminal 526Tyr of FUS for the phosphorylated form, either cytoplasmic or nuclear, and for future screening of FUS$^{p\text{-}Y526}$ interactions with other FUS forms or RBPs that trigger inclusion formation in FTLD and other FUSopathies.

Materials and methods

Plasmid DNA

Full-length wild-type *FUS* was cloned into the pEGFP-C1 vector (Clontech) using the KpnI and BamHI restriction sites to generate N-terminally tagged fusion proteins. The pcDNA3-His$_6$-GFP vector

was generated by inserting the EGFP sequence with a Kozak sequence and the N-terminal His6x tag into the HindIII and KpnI sites of the pcDNA3 vector (Invitrogen). C-terminal fragments of wild-type FUS ($FUS^{490\text{-}Y526}$) and mutated FUS ($FUS^{490\text{-}F526}$) were also cloned into the pcDNA3-His_6-GFP vector with KpnI and BamHI restriction sites to generate His_6-GFP-$FUS^{490\text{-}Y526}$ and His_6-GFP-$FUS^{490\text{-}Y526F}$ constructs, respectively.[26] The pcDNA3 plasmid containing c-Src kinase was obtained from Addgene (#42202).[42] The pcDNA3.1+plasmids with c-Fyn and c-Abl kinase and their constitutively active forms were a kind gift from Dr Wendy Noble (King's College London, London, UK). Sequence integrity of all constructs was verified by sequencing (GATC Biotech).

Custom peptide and antibody production and dot blot analysis

Pairs of phosphorylated and non-phosphorylated peptides corresponding to FUS residues 510-Tyr526 were synthesized. The phosphorylated peptides were then used as immunogens for antibody production in rabbits. Following immunological challenge with the phosphor-FUS peptide, antibodies specific for the phosphorylated Tyr526 peptide (anti-$FUS^{p\text{-}Y526}$) were affinity-purified against the non-phosphorylated Tyr526 peptide. Peptide synthesis and $FUS^{p\text{-}Y526}$ antibody production were performed by AMSBio. For dot blot analysis, non-phosphorylated and phosphorylated FUS peptides [in 0.1% bovine serum albumin (BSA) solution] provided by AMSBio and by Proteogenix (biotinylated) were loaded onto nitrocellulose membrane (GE, Healthcare, Amersham Hybond-ECL) in 10 different dots (volume per dot: 1 μl) at decreasing concentrations 6, 3, 0.3, 0.03, 0.003 μg/μl. The dots were allowed to dry before probing the membranes with anti-$FUS^{p\text{-}Y526}$ and anti-FUS antibodies according to western blotting protocol.

Cell lines and maintenance

HEK293T cells (purchased from ATCC) were maintained in Dulbecco's modified Eagle's medium (DMEM, Gibco) supplemented with 10% foetal bovine serum (ThermoFisher Scientific) and 100 U/ml penicillin-streptomycin (ThermoFisher Scientific) at 37°C in a humidified atmosphere containing 5% CO_2. They were transfected using either PolyJet (SignaGen Laboratories, #SL100688) or Lipofectamine 2000 (Invitrogen) for immunocytochemistry studies, according to the manufacturer's protocol. All of the (co)transfections were carried out side-by-side at the same, to allow comparisons between different experimental conditions. In the kinase inhibition assay, Dasatinib (SML2589, Sigma-Aldrich, 1 and 5 mM stock solutions in DMSO) was added to the cells 1 h before transfection at 0.1, 0.2, 0.5, 1, and 5 μM. Cells were always harvested after 20 h for subsequent analyses.

Neuroblastoma cells SH-SY5Y cell lines (ATCC®CRL-2266™), FlpIn G3BP1 SH-SY5Y generated by us,[43] and the NSC-34 motor neuron-like cells obtained from Cedarlane Laboratories were maintained and differentiated as published.[43-45] Along with mouse primary cortical neurons, these differentiated cells were transfected with 1 μg of c-Src, c-Fyn, or c-Abl plasmid, or in combination with 1 μg of GFP-FUS wild-type plasmid using NeuroMag (OZ Biosciences) according to the manufacturer's instructions. Untransfected differentiated cells/neurons and those transfected with GFP-FUS wild-type only were used as controls. After 24 h of transfection, cells were fixed with 4% PFA for further analysis.

siRNA FUS knockdown

Knockdown of FUS in HEK293T cells using FUS MISSION siRNA (#EHU092111, Sigma-Aldrich), and FLUC MISSION siRNA (#EHUFLUC, Sigma-Aldrich) as a negative control was performed with PepMute siRNA transfection reagent (#SL100566, SignaGen Laboratories) according to manufacturer's protocol. Silenced cells were 48 h transfected again with the same reagent and kinase expressing plasmids and cells were harvested 24 h later. Whole-cell lysates were processed for western blot.

Immunocytochemistry

Cells were grown on poly-L-lysine (Invitrogen, ThermoFisher Scientific) coated glass coverslips in 24-wells. Twenty hours upon (co)transfection, they were washed once with PBS before fixation with 4% paraformaldehyde in PBS for 15 min. Following washing with PBS, cells were permeabilized with 0.1% Triton X-100 in PBS for 15 min. Blocking was performed with 10% donkey serum in PBS. Primary antibodies, diluted in blocking solution were incubated overnight at 4°C. Following three washes with PBS, cells were incubated in the dark with fluorescence-labeled secondary antibodies (anti-mouse Alexa fluor 647 and anti-rabbit Alexa fluor 550, ThermoFisher Scientific) for 1 h at room temperature. After washing with PBS, the cells were stained with DAPI (Sigma-Aldrich), and coverslips were mounted using Prolong Gold reagent (ThermoFisher Scientific). Images were acquired using a Zeiss LSM 710 inverted confocal laser scanning microscope and ZEN 2010 B SP1 software.

Animal husbandry and tissue section preparation

Adult mouse brain tissue was used for cryosectioning. Following a direct cervical dislocation, brains from four 12-week-old male mice (on C57bl6 background) were rapidly removed, sharply divided into four pieces of equal size, and placed into 4% paraformaldehyde in PBS for 30 min on ice. The brain pieces were then embedded into OCT (Tissue Tek, Sakura Finetek Europe B.V.), frozen in liquid nitrogen and sectioned into 10-μm-thick frozen fixed sections in a cryostat (Leica) at −20°C, collected on SuperFrost Plus slides (Menzel-Glaaser) and air-dried before further processing.

In parallel, we used paraffin sections (FFPE) of formalin-fixed material from $n = 3$, 50-week-old male wild-type animals (three sections, each for every brain region/probe) for additional histological analyses. Here, the freshly dissected whole brains were immediately fixed in 4% formalin for 48 h and then processed for paraffin embedding.

Immunohistochemistry of mouse brain

Immunohistochemistry protocol of formalin-fixed, paraffin embedded tissue was the same as used for human tissue (see the 'Immunofluorescence labelling of human post-mortem tissue' section). However, frozen fixed sections prepared from mouse brains were rehydrated with PBS for 20 min and treated with 0.4% Triton in PBS for 10 min at room temperature. For immunofluorescence, non-specific labelling was blocked by 2% BSA (Sigma-Aldrich) in PBS for 1 h at room temperature. Then, the sections were incubated overnight at 4°C with the following primary antibodies: anti-$FUS^{p\text{-}Y526}$ (1:500, AMSBio), anti-FUS (1:300, Sigma-Aldrich), anti-pSrc, anti P-Fyn (both 1:500, Santa Cruz), anti-NeuN (1:200, MAB377, Millipore), anti-GFAP (1:100), anti-A3B5 (hybridoma supernatant, 1:200), and anti-SMI33 (1:1000, Sternberger Monoclonals). After washing with PBS, sections were

incubated with secondary antibodies conjugated with Alexa fluor 488 or 647 (1:1000, Cell Signaling) for 1 h at room temperature in the dark. A series of negative controls were performed, omitting the primary antibody. Sections were washed and mounted in ProLong Gold Antifade reagent (ThermoFisher Scientific). Slides were examined with a Zeiss LSM 710 inverted confocal laser scanning microscope and ZEN 2010 B SP1 software.

Human post-mortem tissue

Post-mortem tissues were obtained within 6–30 h after death (Supplementary Table 1). Human post-mortem brain (frontal cortex) samples fixed in buffered formalin ($n = 4$ FTLD-FUS patients and $n = 4$ age-matched controls) were obtained from the archives of the Department of Neuropathology, Amsterdam UMC, University of Amsterdam, and the Netherlands Brain Bank (NBB). The controls included in the present study were adult individuals without any history of neurological disease, based on their last clinical evaluation. The demographic details of the FTLD-FUS patients together with the normal non-neurological controls included in this study are summarized in Supplementary Table 1.

Immunofluorescence labelling of human post-mortem tissue

Double immunofluorescence labelling was performed as described previously.[46,47] In brief, deparaffinized tissue sections were boiled in citrate buffer, pH 6 (Dako), for 20 min in a pressure cooker for antigen retrieval. Sections were blocked with 10% normal goat serum (Life Technologies) for 1 h at room temperature and incubated with the required primary antibody ($FUS^{p\text{-}Y526}$ and FUS, pAbl; dilutions 1:100 for each antibody) at 4°C overnight. After washing in TBST for 10 min, the sections were incubated with Alexa conjugated secondary antibody (dilution, 1:500 in PBS) at room temperature for 2 h. Sections were washed in TBST (2 × 10 min) and stained for 10 min with 0.1% Sudan Black in 80% ethanol to suppress endogenous lipofuscin auto-fluorescence and then washed for 5 min in TBST and mounted with Vectashield mounting medium (Vector Laboratories) containing DAPI. Images were obtained with a laser scanning confocal microscope (LSM 700; Zeiss) using 40× and 63× objectives (Zeiss). Images were acquired by averaging four scans per area of interest resulting in an image size of 1024 × 1024 pixels. For quantification only high-resolution images were used. The laser intensity was kept constant for all of the sections examined. Images were analysed using ZEN (Blue edition) 2009 and ImageJ software. One section per each individual control ($n = 4$) and FTLD case ($n = 4$) was examined per each double staining $FUS^{p\text{-}Y526}$/FUS and $FUS^{p\text{-}Y526}$/pAbl. Per section, at least six visual fields were imaged, each containing 6–12 neurons. Six of the sharpest neuron images (best nuclear resolution) were analysed from each image for nuclear to cytoplasmic $FUS^{p\text{-}Y526}$, FUS, and pAbl ratio. Altogether, for the nucleo/cytoplasmic ratio of each (FUS and pAbl), approximately 140 control and 140 FTLD neurons were examined, whereas the $FUS^{p\text{-}Y526}$ ratio was examined in more than 250 neurons.

Further details of antibodies, primary mouse cortical neuron culture preparation, western blot analyses, His-tag pull-down, immunoprecipitation analyses, phosphatase assay, diaminobenzidine (DAB) immunohistochemistry, induction of stress granule formation in FlpIn SH-SY5Y cells and prediction analyses for FUS tyrosine phosphorylation can be found in the Supplementary material.

Statistical analyses

Quantifications of FUS and $FUS^{p\text{-}Y526}$ nuclear/cytoplasmic localization were performed using ImageJ software (National Institutes of Health, Baltimore, MD). Obtained fluorescence signals were adjusted by subtraction of the mean background levels of the cell slide. The signal intensity (for FUS and $FUS^{p\text{-}Y526}$) was defined as the average of the intracellular cytoplasmic or nuclear signal intensities of the individual cell (demonstrated positive for wild-type and truncated FUS transfection—GFP signal and overlapping with pFUS signal). Data were analysed using GraphPad Prism 6 (GraphPad Software). Differences between the two groups were analysed using Student's *t*-test (0.05 threshold value). Where differences between multiple groups were analysed, one-way ANOVA followed by a Bonferroni *post hoc* test was used to assess which groups were significantly different (0.05 threshold value).

Ethical approval

All procedures involving human participants, including the use of post-mortem tissue samples, were performed in accordance with the ethical standards of the institutional and/or national research committee as well as with the 1964 Helsinki declaration and its later amendments. The studies were approved by the Ethical Committees of the Academic Medical Center, Amsterdam (W11 073).

Ethical statement

The animal facilities in our department at J. Stefan Institute were approved by the decree UVHVVR, OU Ljubljana No. U34401-24/2013/9, date 30.10.2013, allowing to breed laboratory mice. The study was approved by the Slovenian National Medical Ethics Committee (Approval No. U34401-12/2014/4).

Data availability

The authors confirm that the data supporting the findings of this study are available within the article and its Supplementary material.

Results

Confirmation of specificity and detection of Tyr526 FUS phosphorylation with the $FUS^{p\text{-}Y526}$ antibody

Two pairs of FUS and $FUS^{p\text{-}Y526}$ antibodies were raised in rabbits against the last 16 amino acid residues of the FUS protein with non-phosphorylated (FUS) or phosphorylated C-terminal 526Tyr residue ($FUS^{p\text{-}Y526}$) from AMSBio. They were affinity purified, and their specificity for detection of total and 526Tyr-phosphorylated FUS was verified by dot blots using the synthetic peptides with unphosphorylated and phosphorylated C-terminal tyrosine (Supplementary Fig. 1A). The specificity of the $FUS^{p\text{-}Y526}$ antibody for the phosphorylated 526Tyr residue was confirmed by the complete absence of the $FUS^{p\text{-}Y526}$ signal in the samples containing non-phosphorylated peptides. Moreover, $FUS^{p\text{-}Y526}$ signal was specifically observed only in total protein lysates from HEK293T cells transfected with c-Src and c-Abl kinases (Supplementary Fig. 1B–G). In screening of these lysates with antibodies against TAF15, SAM68, hnRNPA1, and EWSR1, RBPs that share the –PY-NLS in their sequence (Supplementary Fig. 1C), no band was detected near the predicted

molecular weight of the FUS$^{p\text{-}Y526}$ signal (Supplementary Fig. 1D–G), implying the specificity of FUS$^{p\text{-}Y526}$ antibody to FUS.

Src-family kinases (c-Src, c-Fyn, and c-Abl) showed the highest probability scores (Fig. 1A) in the Web-based prediction programs NetPhos, DisPhos and BioCuckoo (see Supplementary material for details) when screening the FUS protein sequence for candidates to catalyse Tyr526 FUS phosphorylation. These kinases were found to be causative for the appearance of the shifted FUS$^{p\text{-}Y526}$ band in kinase transfected cells (Fig. 1B) observed by ourselves and others,[13,33] and explained either by Src-distributive versus Abl-processive mode of action[48,49] or the formation of higher-order FUS complexes.[13,15,26,33,50] Pretreatment with dasatinib, a known inhibitor of Src/Abl kinases,[51] decreased FUS$^{p\text{-}Y526}$ signal intensity in c-Src (Fig. 1C), c-Fyn (Fig. 1D), and c-Abl (Fig. 1E) transfected cells in a concentration dependent manner. Intracellular localization of FUS$^{p\text{-}Y526}$ signal by immunocytochemistry revealed predominantly nuclear FUS$^{p\text{-}Y526}$ staining in the c-Src and c-Fyn transfected cells, whereas cytoplasmic FUS$^{p\text{-}Y526}$ staining was detected in the c-Abl transfected HEK293T cells (Supplementary Fig. 2A). Because co-immunostaining of transfected cells with plasmids encoding constitutively active (phosphorylated) forms of kinases (pSrc, pFyn, and pAbl) and FUS$^{p\text{-}Y526}$, increased FUS$^{p\text{-}Y526}$ immunoreactivity (intensity in kinase transfected cells, Supplementary Fig. 2B), resulting in increased and decreased FUS$^{p\text{-}Y526}$ nuclear-to-cytoplasmic ratio when compared to wild-type kinase transfected cells (Supplementary Fig. 3A–C), these mutant kinase plasmids were used thereafter.

To ascertain that the FUS$^{p\text{-}Y526}$ signal observed in cells was derived from phosphorylated C-terminal Tyr526 FUS, the N-terminally His_6-GFP tagged C-terminal fragment of FUS (35 amino acid residues),[26] ending in either Tyr (GFP-FUS$^{490\text{-}Y526}$) or Phe (GFP-FUS$^{490\text{-}Y526F}$), was expressed in HEK293T cells along with c-Src, c-Fyn, and c-Abl kinase (Fig. 2A). Western blot confirmed the absence of the GFP-FUS$^{490\text{-}pY526}$ band in cells expressing FUS$^{490\text{-}Y526F}$, with only the endogenous FUS$^{p\text{-}Y526}$ band detected by the FUS$^{p\text{-}Y526}$ antibody, and His-tag pull-down analysis confirmed that the 30-kDa GFP-FUS$^{490\text{-}pY526}$ band belongs to the C-terminal fragment of GFP-FUS$^{490\text{-}Y526}$ (Fig. 2B). Additionally, *in vitro* phosphatase assays (Fig. 2C and D) and siRNA FUS silencing (Fig. 2E) were performed. Phosphatase (CIP) treatment of lysates (non-transfected, kinase-transfected, and kinase/GFP-FUS$^{490\text{-}Y526}$ co-transfected cells) and FUS-siRNA silencing of cells transfected with any of the three kinases (Src, Fyn, Abl) resulted in abrogation of the endogenous FUS$^{p\text{-}Y526}$ band (Fig. 2C–E) and the C-terminal GFP-FUS$^{490\text{-}pY526}$ band (Fig. 2D). Finally, the specificity of the FUS$^{p\text{-}Y526}$ antibody for FUS$^{p\text{-}Y526}$ and GFP-FUS$^{490\text{-}pY526}$ was confirmed by immunoprecipitation with anti-FUS$^{p\text{-}Y526}$, anti-FUS (NB100-565), anti-GFP antibodies, and IgG antibody as control, followed by FUS$^{p\text{-}Y526}$, FUS, pTyr (Supplementary Fig. 4A–D) and other PY-NLS proteins (TAF15, SAM68, EWSR1, hnRNPA1) immunoblot detection (Supplementary Fig. 5A–D).

Phosphorylation of Tyr526 FUS affects FUS solubility in a kinase-dependent manner

Because increased cytoplasmic FUS localization may lead to FUS aggregation, the effect of the kinases c-Src, c-Fyn, and c-Abl on endogenous FUS solubility was analysed by biochemical fractionation of cell lysates. Western blot analyses of RIPA, UREA-soluble, and UREA-insoluble fractions showed that c-Src and c-Fyn phosphorylated FUS$^{p\text{-}Y526}$ was mainly found in the soluble fractions, whereas c-Abl phosphorylated FUS$^{p\text{-}Y526}$ was only found in the insoluble fraction (Supplementary Fig. 6A), suggesting that c-Abl mediated FUS phosphorylation affects the solubility and aggregation of FUS. Non-phosphorylated FUS was found mainly in the RIPA soluble fraction, with traces in the UREA fraction, and was absent in the insoluble fraction. Here, commercial antibody raised against middle region of FUS (mouse monoclonal antibody SAB4200478) proved incapable of detecting FUS$^{p\text{-}Y526}$ in a western blot; Supplementary Fig. 6A). Consistently, immunocytochemical staining with the antibody mentioned above and other commercial rabbit polyclonal antibodies NB100-565 (against a 1–50 amino acid epitope of FUS) and NB100-561 (against a 400–450 amino acid epitope of FUS) (Supplementary Fig. 7) demonstrated that only the rabbit antibody NB100-565 (Supplementary Fig. 7A), and the mouse antibody SAB4200478 (Supplementary Fig. 7C) could detect increased levels of FUS in c-Src, c-Fyn and c-Abl transfected cells. It has been shown that phosphorylation of Tyr526 FUS in cells is compensated by increased FUS expression,[33,52] which is also suggested by antibodies binding to FUS$^{p\text{-}Y526}$ and immunoprecipitation assays. This also meant that the N-terminal region in FUS$^{p\text{-}Y526}$ remained accessible for antibody binding (NB100-565), whereas the accessibility of the internal 400–450 amino acid epitope recognized by NB100-561 may have been abolished by Tyr phosphorylation (Supplementary Fig. 7B).

For additional analyses of the effect of phosphorylation of Tyr526 on endogenous FUS solubility, the plasmid encoding wild-type GFP-FUS was used in kinase co-expression experiments in HEK293T cells (Fig. 3A–D), primary mouse cortical neurons (Fig. 3E), and differentiated SH-SY5Y and NSC34 cells (Supplementary Fig. 8A–D). To ascertain that in these cells detected FUS$^{p\text{-}Y526}$ signal indeed arises from phosphorylated Tyr526 of FUS, HEK293T cells were also examined for the co-expression of the pSrc, pFyn and pAbl kinases with plasmids encoding C-terminal fragment His_6-GFP-FUS$^{490\text{-}Y526}$ and the plasmid encoding full-length mutant FUS in which all 35 but the last 526 Tyr are replaced by Phe (Myc-FUSall526Y) (Supplementary Fig. 9A and B). Co-expression of GFP-FUS, His_6-GFP-FUS$^{490\text{-}Y526}$ and Myc-FUSall526Y and constitutively active pSrc, pFyn, and pAbl kinases showed enhanced cytoplasmic localization and aggregation of FUS$^{p\text{-}Y526}$ only in cells co-transfected with a cAbl expressing plasmid (lower panels in Fig. 3A and B and Supplementary Figs 8 and 9), whereas in cells expressing active pSrc and pFyn kinases mainly nuclear FUS$^{p\text{-}Y526}$ signal was observed. Although FUS$^{p\text{-}Y526}$ signal in co-transfected cells was expected to derive from both phosphorylated endogenous FUS and GFP/myc-tagged FUS, complete overlap between FUS$^{p\text{-}Y526}$ and GFP/Myc signal was not observed. Therefore, the enhanced cytoplasmic aggregation of FUS$^{p\text{-}Y526}$ could also be due to phosphorylation of endogenous FUS, its cytoplasmic localization, and entanglement with overexpressed FUS forms. Sequestration of wild-type FUS into the cytoplasmic aggregates by overexpressed mutant FUS has been shown previously by us and others.[2,53] Image quantification analyses also confirmed the increase of the cytoplasmic FUS$^{p\text{-}Y526}$ signal in cells co-transfected with c-Abl compared with c-Src and c-Fyn (see changes in nuclear to cytoplasmic ratio) (Fig. 3C and D). In GFP-FUS and c-Abl co-transfected cells also, increased intensity of FUS signal was detected in the cytoplasm, possibly explaining the observed increased cytoplasmic FUS aggregation and compaction (Fig. 3B and E). Although in additional cell models, differentiated SH-SY5Y (Supplementary Fig. 8A and B) and differentiated NSC-34 cells (Supplementary Fig. 8C and D) co-transfected with GFP-FUS and kinases, the patterns of subcellular FUS$^{p\text{-}Y526}$ signal localization were similar to those observed in co-transfected HEK293T cells (Fig. 3A

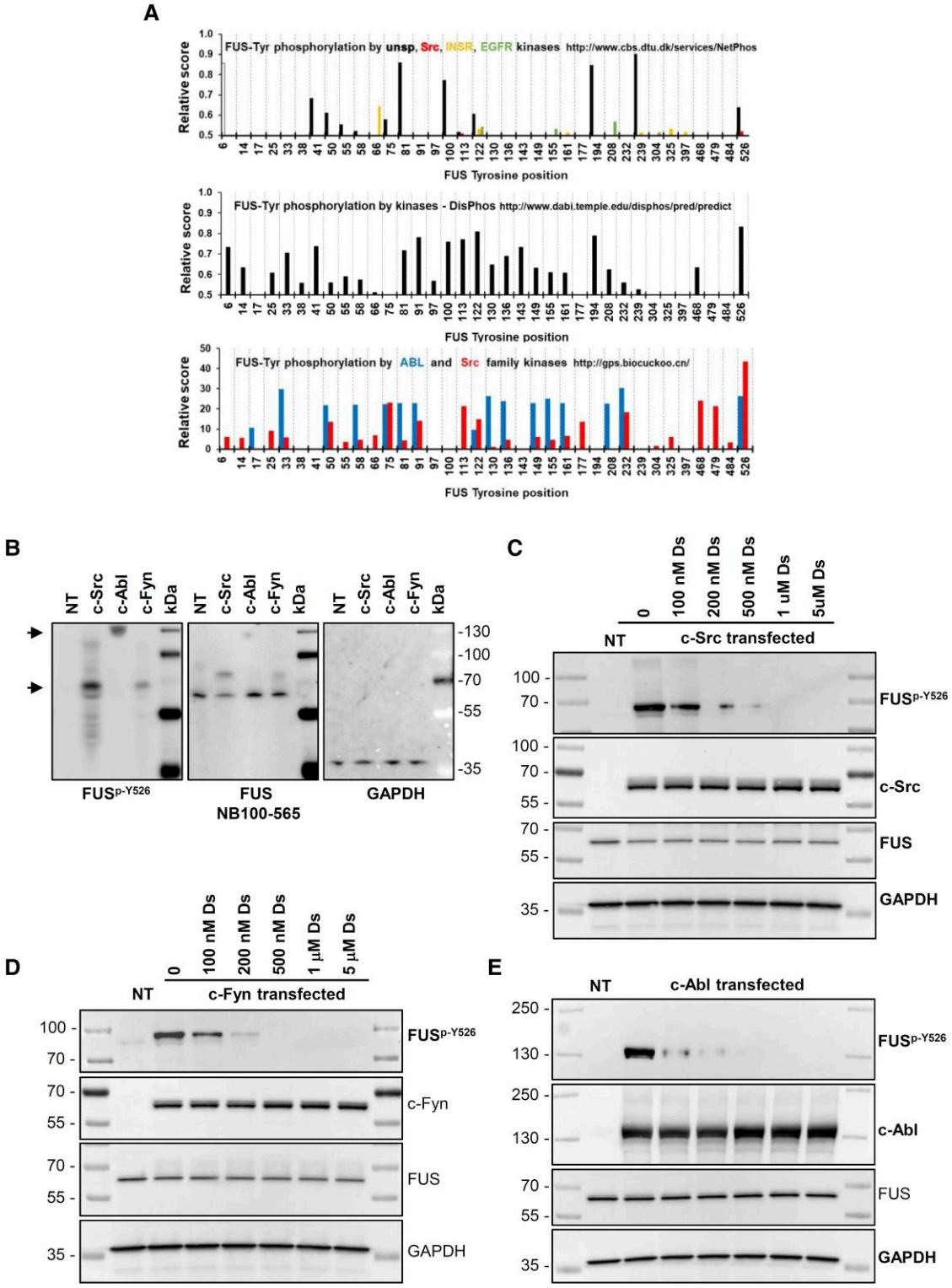

Figure 1 Members of src family kinases (c-src, c-fyn, c-abl) phosphorylate the c-terminal Tyr526 of FUS. (**A**) Web prediction programmes NetPhos (*top*), DisPhos (*middle*), and BioCuckoo (*bottom*) were run to search for Tyr526 phosphorylating kinase candidates and kinases (c-Src, c-Fyn, and c-Abl) of Src-family (SFK) revealed as most probable candidates. (**B**) The phosphorylated target protein of all three SFK was detected with FUS$^{p\text{-}Y526}$ Ab (*left*) at the shifted position compared to the FUS band detected with NB100-565 (*middle*), and GAPDH (*right*). Dasatinib, an SFK inhibitor, inhibited the activity of expressed wild-type kinases (**C**) c-Src, (**D**) c-Fyn, and (**E**) c-Abl and decreased the signal of FUS$^{p\text{-}Y526}$ in cell lysates in a concentration-dependent manner.

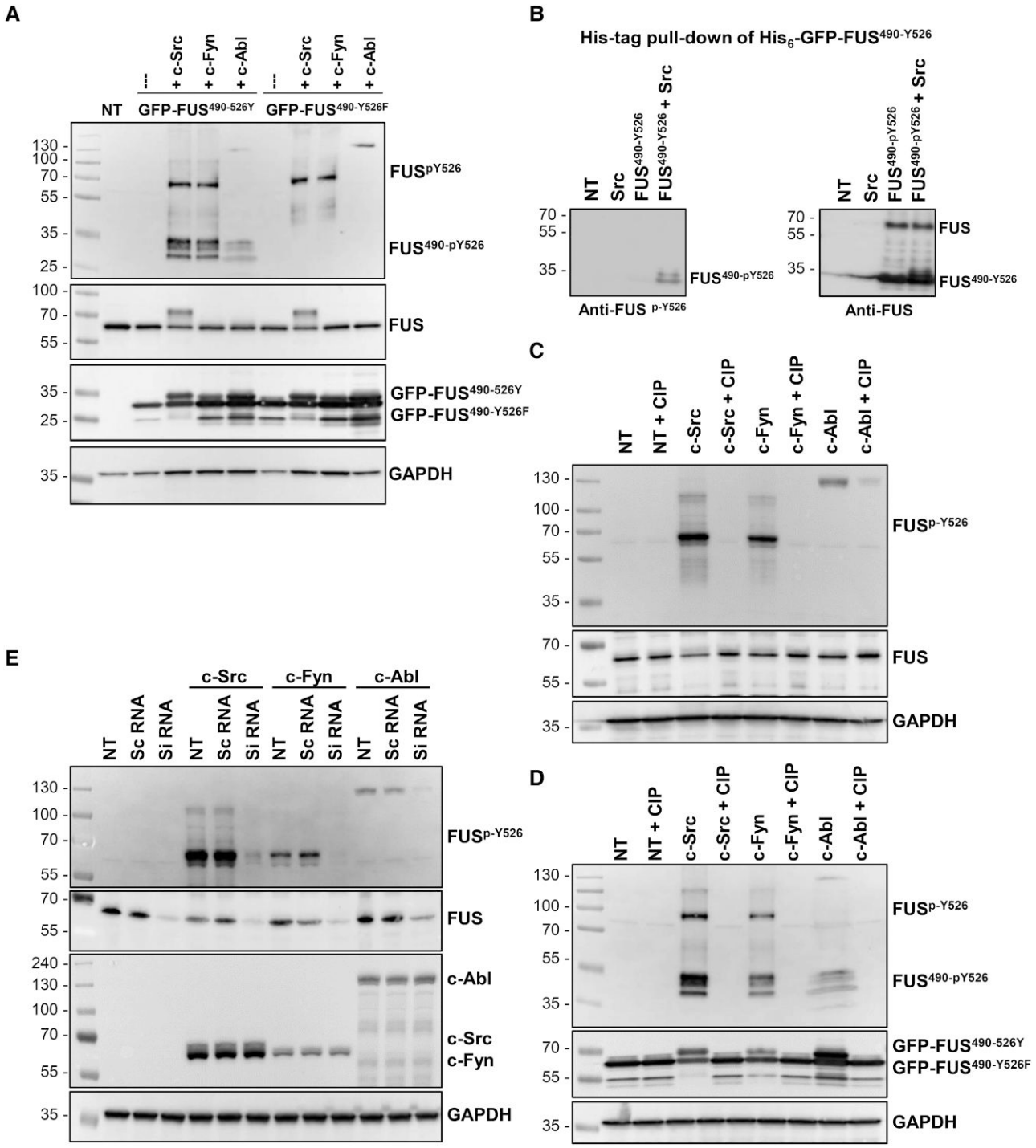

Figure 2 The specificity of FUS$^{p\text{-}Y526}$ antibody was confirmed by *in vitro* phosphatase assay and FUS knockdown studies in HEK293T cells. (**A**) The C-terminal (His$_6$-GFP-FUS^{490}–^{526Y}, His$_6$-GFP-FUS$^{490\text{-}Y526P}$) fragments of FUS containing either Tyr or Phe as the last residue were expressed together with constitutively active kinases in HEK293T cells, and the lysates were immunoblotted against FUS$^{p\text{-}Y526}$, FUS, GFP, and GAPDH. (**B**) His-tag pull-down of His$_6$-GFP-FUS^{490}–^{526Y} from NT, kinase-transfected and kinase/His$_6$-GFP-FUS^{490}–^{526Y} co-transfected cell lysates, immunoblotted against FUS$^{p\text{-}Y526}$ (*left*) and FUS (*right*). (**C**) The lysates of non-transfected and c-Src, c-Fyn, and c-Abl transfected HEK293T cells and (**D**) the lysates of non-transfected, His$_6$-GFP-FUS$^{490–526Y}$ and kinase co-transfected HEK293 cells were subjected to calf intestinal phosphatase activity and analysed by western blot for the FUS$^{p\text{-}Y526}$, which decreased in the phosphatase treated samples. (**E**) Knockdown of FUS by siRNA was performed in HEK293T cells and then transfected with either c-Src, c-Fyn, or c-Abl to induce Tyr526 FUS phosphorylation. Western blots with anti- FUS$^{p\text{-}Y526}$, FUS, c-Abl, c-Src, and c-Fyn antibodies showed the specificity of the FUS$^{p\text{-}Y526}$ antibody.

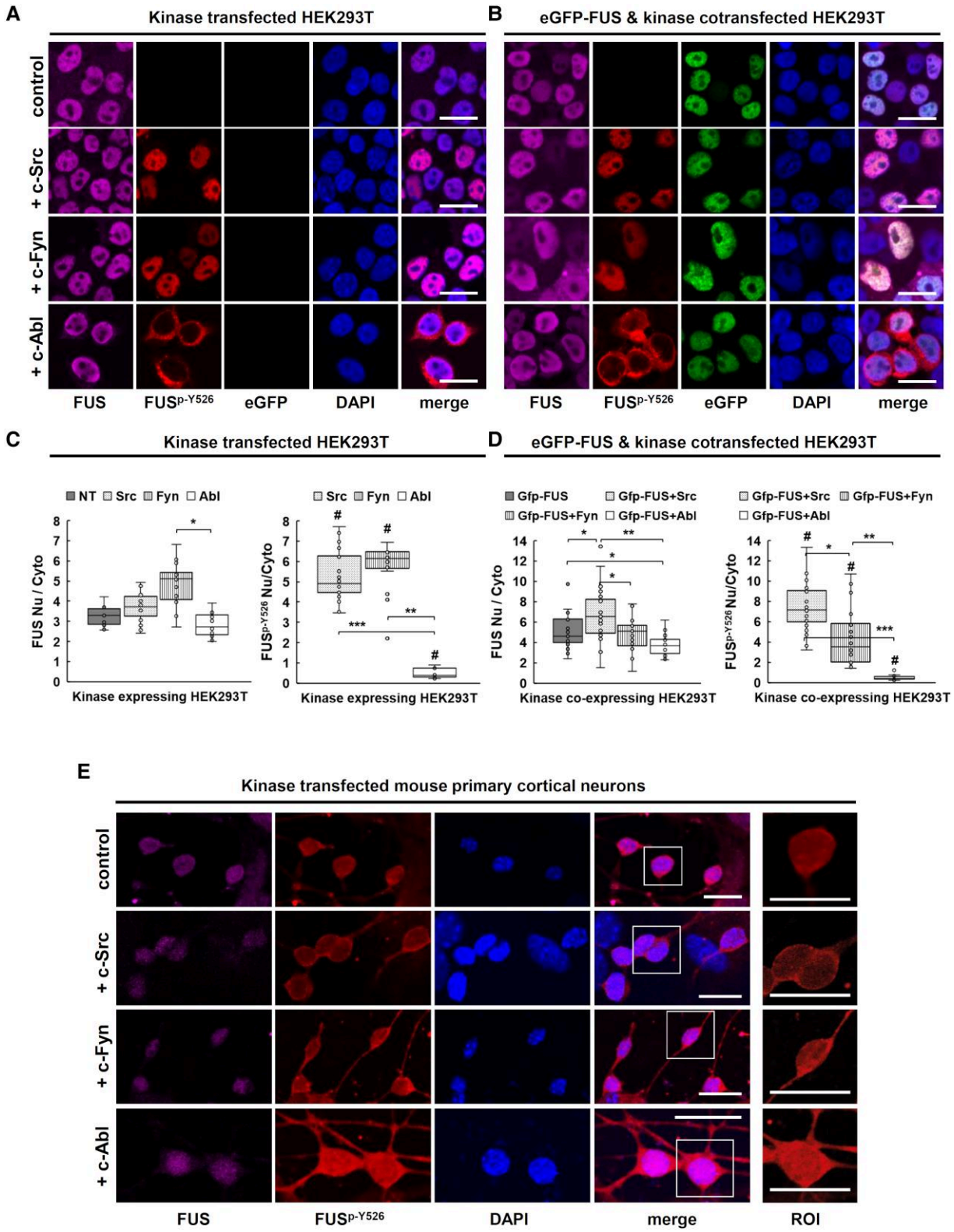

Figure 3 Kinases affect localization and aggregation of non-phosphorylated and phosphorylated Y526 FUS. HEK293T cells were transfected with (**A**) constitutively active c-Src, c-Fyn, and c-Abl expression plasmids and co-transfected with (**B**) constitutively active kinases and a GFP tagged full-length FUS (green). (**C** and **D**) Quantitative assessment of nuclear and cytoplasmic FUS (magenta) and FUS$^{p\text{-}Y526}$ (red) signal was performed using ImageJ and the ratio of nuclear to cytoplasmic FUS and FUS$^{p\text{-}Y526}$ signals in positively transfected cells was determined alongside their relative cytoplasmic abundance. (**E**) The culture of mouse primary cortical neurons was established, and neurons were transfected with active kinases. Cell nuclei were counterstained with DAPI (blue). One-way ANOVA, $^{*}P < 0.05$, $^{**}P < 0.01$, $^{***}P < 0.001$. Scale bars = 20 μm in **A** and **B**; 15 μm in **E**. ROI = region of interest.

and B), this was not confirmed in primary mouse cortical neurons (Fig. 3E). Unlike other cells, control mouse primary cortical neurons demonstrated positive for FUS$^{p\text{-}Y526}$ and transfection with both Src and Fyn kinase had no apparent effect on nuclear and cytoplasmic content, whereas Abl expression appeared to enhance FUS$^{p\text{-}Y526}$ immunoreactivity in both cytoplasm and nucleus (Fig. 3E). Overall, this suggests a kinase-specific effect on full-length FUS, possibly leading to differential FUS aggregation and formation of FUS aggregates of different toxicity in (non-)differentiated cells and primary neurons.

Phosphorylated Tyr526 FUS is detected in mouse neurons and co-localizes with active kinases

Because the kinases studied here can be activated by different environmental stimuli, this opened the possibility that the dynamics of aggregate formation and the severity of neurodegeneration are mediated in part by Src and Abl. To verify the immunoreactive pattern of FUS$^{p\text{-}Y526}$ in cells *in vivo*, transverse frozen-fixed and paraffin-embedded (FFPE) tissue sections were prepared from the brains of male wild-type mice and labelled for the presence of FUS$^{p\text{-}Y526}$ (Fig. 4A–D). FUS$^{p\text{-}Y526}$ staining was detected in a subset of astrocytes (Fig. 4A) and in neuronal cells of the cerebral cortex (Fig. 4B), Purkinje cells of the cerebellum (Fig. 4C), and neurons of the hippocampus and brainstem (Fig. 4D and E).

To test whether the FUS$^{p\text{-}Y526}$ signal detected in brain cells *in vivo* is associated with active Src family kinases, we next performed co-labelling using anti-FUS$^{p\text{-}Y526}$, anti-pSrc, anti-pFyn, and anti-pAbl antibodies (Fig. 5) on mouse brain sections. Interestingly, we observed an overlapping pattern of immunoreactivity of FUS$^{p\text{-}Y526}$ and active kinases (pSrc, pFyn, p-Abl) in neuronal cells in the hippocampus (Fig. 5A). Conversely in the brainstem, only the overlapping pattern of FUS$^{p\text{-}Y526}$ and pSrc immunoreactivity was observed (Fig. 5B), whereas in the frontal cortex, the immunoreactivity patterns of both pSrc and pAbl also strongly overlapped with FUS$^{p\text{-}Y526}$ immunoreactivity (Fig. 5C). This suggests differential activity of Src-family kinases in neuronal cells *in vivo* in mice, possibly correlating with the detection of FUS$^{p\text{-}Y526}$ immunoreactivity.

Phosphorylated Tyr526 FUS reveals altered nucleo-cytoplasmic localization in FTLD-FUS brain

Impaired nucleo-cytoplasmic localization of FUS and its presence in the form of insoluble cytoplasmic aggregates within affected neurons are common features in FTLD-FUS patients. We have previously reported that phosphorylation of Tyr526 FUS inhibits the binding of FUS to its nuclear importer TNPO1, thereby enhancing its cytoplasmic mislocalization.[26] Interestingly, we observed significant co-localization of pAbl kinase together with FUS$^{p\text{-}Y526}$ in the normal frontal cortex of wild-type mice (Fig. 5C). Considering that the frontal cortex is severely affected in FTLD-FUS patients, we expected changes in the immunolabelling patterns of FUS$^{p\text{-}Y526}$ in FTLD-FUS patients compared with controls. Thus, we next analysed the immunolabelling patterns of pAbl and FUS$^{p\text{-}Y526}$ in post-mortem frontal cortex tissue obtained from a well-characterized cohort of FTLD-FUS patients (Figs 6 and 7 and Supplementary Table 1). DAB immunohistochemistry performed with our specific anti-FUS$^{p\text{-}Y526}$ antibody revealed diffuse nuclear and cytoplasmic immunoreactivity in FUS$^{p\text{-}Y526}$ cortical neurons from controls (Fig. 6A), whereas a peculiar, atypical pattern of pronounced granular and small globular FUS aggregation was observed in many cortical neurons from FTLD-FUS cases (Fig. 6A, black arrows). In many neurons, we also observed cytoplasmic granular accumulations (Fig. 6A, white arrow). Double immunolabelling with FUS$^{p\text{-}Y526}$ and FUS antibody was even more sensitive and confirmed this exciting pattern of immune reactivities. Consistent with DAB immunohistochemistry, several cortical neurons (10–20%) in FTLD-FUS showed granular cytoplasmic accumulation of FUS$^{p\text{-}Y526}$ (Fig. 6B), which rarely and only partly co-localized with cytoplasmic FUS aggregates (15–20%) detected with commercial FUS antibody (Novus) (Fig. 6C, white arrow). Apart from cytoplasmic atypical granular FUS$^{p\text{-}Y526}$ accumulation, the majority (50–60%) of FTLD-FUS cortical neurons consistently showed strong nuclear FUS$^{p\text{-}Y526}$ immunoreactivity compared with normal control cortical neurons (Fig. 6D and E). Interestingly, FUS$^{p\text{-}Y526}$ immunolabelling was more intense in FTLD-FUS cortical neurons at the nuclear membrane (Fig. 6C). These results were further verified by ImageJ quantification (Fig. 6E and F) and line scans (Supplementary Fig. 10A–C).

To further our understanding of the phosphorylation of Tyr526 FUS by Src family kinases, we examined the immunoreactivity pattern of pAbl and FUS$^{p\text{-}Y526}$ (Fig. 7). Activated cAbl kinase has been repeatedly associated with neurodegenerative diseases, in which its abnormal activation has been shown to be increased in brain neuronal cells.[39] Consistent with the previously observed immunoreactivity of FUS$^{p\text{-}Y526}$ (Fig. 6), we again observed a similar pattern of increased FUS$^{p\text{-}Y526}$ immunoreactivity together with similarly increased immunolabelling of pAbl in the nucleus in the cortical neurons of FTLD-FUS patients (Fig. 7A–C). Quantification analysis revealed an increased nuclear-to-cytoplasmic ratio of pAbl signal intensity in cortical neurons from FTLD-FUS (Fig. 7B). To gain insight into how increased Abl activity might affect the subcellular distribution of FUS$^{p\text{-}Y526}$ under stress conditions, we generated FlpIn SH-SY5Y cells expressing the mScarlet-G3BP1 protein, a known component of stress granules. These were transfected with c-Abl and subjected to oxidative stress conditions by treatment with 50 μM arsenite (Fig. 8). As in previous cell models, with the exception of primary mouse cortical neurons, predominantly cytoplasmic FUS$^{p\text{-}Y526}$ signal was observed only in c-Abl transfected cells, where FUS$^{p\text{-}Y526}$ were sequestered in G3BP1-positive stress granules after arsenite treatment. In summary, our results suggest a disruption of the nucleocytoplasmic shuttling mechanism of FUS in FTLD, likely caused by stress and cell compartment-specific activity of pAbl kinase, which has been shown to phosphorylate Try526 FUS, and therefore may underlie the markedly different appearance and progress of FTLD compared with other neurodegenerative FUSopathies.

Discussion

Fibrillar FUS aggregates are the major pathological entity in affected neurons in the brains of FTLD-FUS and ALS-FUS patients.[54] When its well-regulated nucleocytoplasmic shuttling is disrupted, elevated levels of cytoplasmic FUS result in abnormal FUS accumulation in cytoplasmic inclusions[55] and toxic gain-of-function.[56] However, there are differences between FTLD-FUS and ALS-FUS in the composition of cytoplasmic FUS inclusions. The FUS aggregates in FTLD-FUS consist of wild-type FUS, other FET proteins, and TNPO1, a known nuclear importer of FUS, whereas the FUS aggregates in ALS-FUS always consist of mutant and sequestered FUS only, without TNPO1,[57] suggesting differences in the mechanism of cytoplasmic FUS localization in the two diseases. We already showed that phosphorylation of Tyr526 FUS (FUS$^{p\text{-}Y526}$) by c-Src family kinases enhances cytoplasmic localization of FUS and

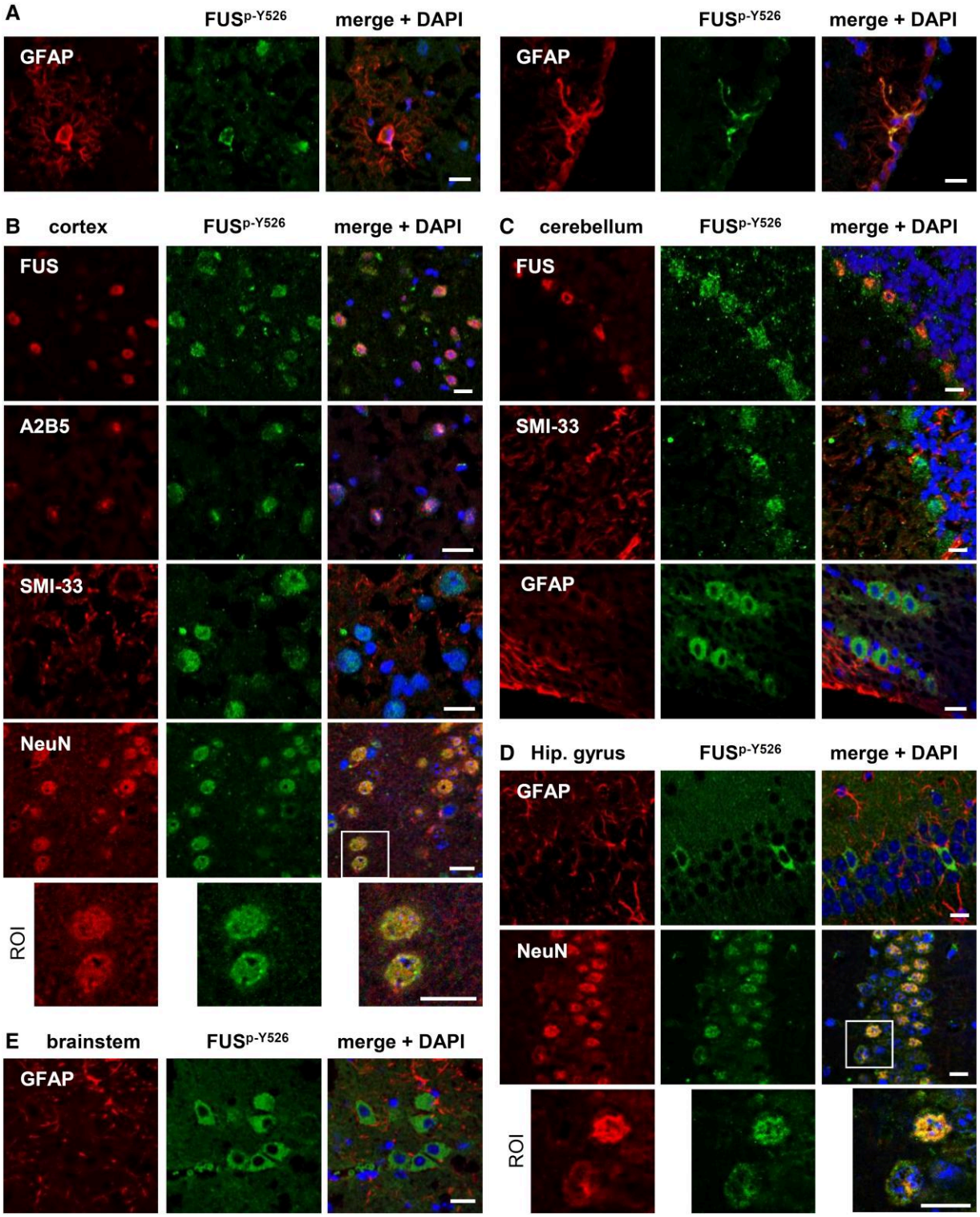

Figure 4 FUS$^{p\text{-}Y526}$ is detected *in vivo* in mouse brains. Immunocytochemical analyses performed on transverse frozen-fixed and paraffin-embedded tissue sections of mouse brain showed sparse detection of FUS$^{p\text{-}Y526}$-positive cells (green) throughout brain tissue, in (**A**) astrocytes co-stained for GFAP (red), (**B**) Pyramidal neurons of the cerebral cortex co-stained for A2B5 (red), SMI33 and NeuN proteins (red), and (**C**) Neurons in the cerebellum co-stained for SMI-33. (**D**) No co-localization of FUS$^{p\text{-}Y526}$ and GFAP was observed in the neurons or in (**E**) brainstem. The neuronal nuclei were counter-stained with DAPI. NeuN/FUS$^{p\text{-}Y526}$ = paraffin sections; others = frozen-fixed sections. Scale bar = 15 μm.

inhibits binding of TNPO1,[26] which is required for FUS nuclear import[28,30,31] and detachment of FUS molecules from early soluble FUS aggregates.[31] Hence, our hypothesis here was that, similar to methylation,[58] phosphorylation of Tyr526 FUS may play a role in cytoplasmic FUS aggregation in FTLD-FUS, particularly by increasing cytoplasmic levels of wild-type FUS and mediating formation

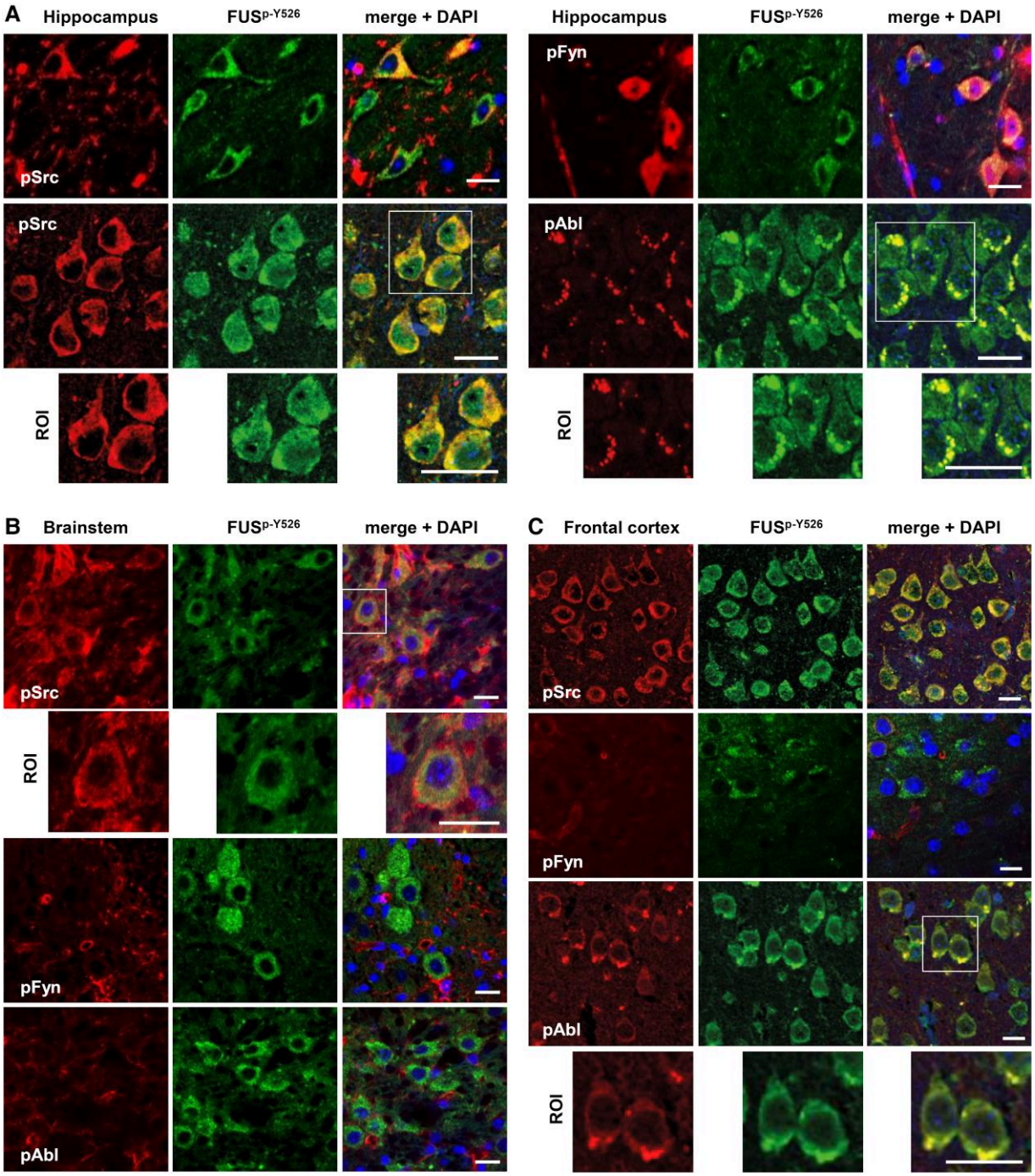

Figure 5 ***In vivo*** **FUS$^{p\text{-}Y526}$ signal overlaps with the expression of active src family kinases and appears brain region-specific.** Frozen-fixed and paraffin sections of brain from wild-type mice were co-immunostained for active phosphorylated pSrc, pFyn, pAbl and FUS$^{p\text{-}Y526}$, and co-localization of signals was observed in neurons of (**A**) hippocampus, (**B**) brainstem, and (**C**) frontal cortex. Frozen-fixed sections = pFyn/FUS$^{p\text{-}Y526}$; paraffin sections = pAbl/pSrc/FUS$^{p\text{-}Y526}$. Scale bar = 15 μm.

of its early cytoplasmic aggregates. To gain insight into Tyr526 FUS phosphorylation we developed an antibody that specifically recognizes phosphorylated Tyr526 FUS (FUS$^{p\text{-}Y526}$) and used it in *in vitro* cell/lysate and *in vivo* brain labelling.

In this way, we first demonstrated that the level of Tyr526 FUS phosphorylation and its protein-protein binding properties are kinase-type dependent. By siRNA silencing, phosphatase assay, and immunoprecipitation we confirmed the high specificity of our FUS$^{p\text{-}Y526}$ antibody. Although several types of Src-family kinases are activated by stress associated with the development of neurodegenerative diseases,[13,32] we confirmed that both predicted (http://gps.biocuckoo.cn/) kinases c-Abl and c-Src phosphorylate Tyr526 FUS at increased levels compared to c-Fyn kinase as also observed by others.[59] The FUS$^{p\text{-}Y526}$ band shift we observed in lysates from kinase-expressing cells was consistent with previously observed multiple Tyr- or Ser/Thr-phosphorylated FUS, which are

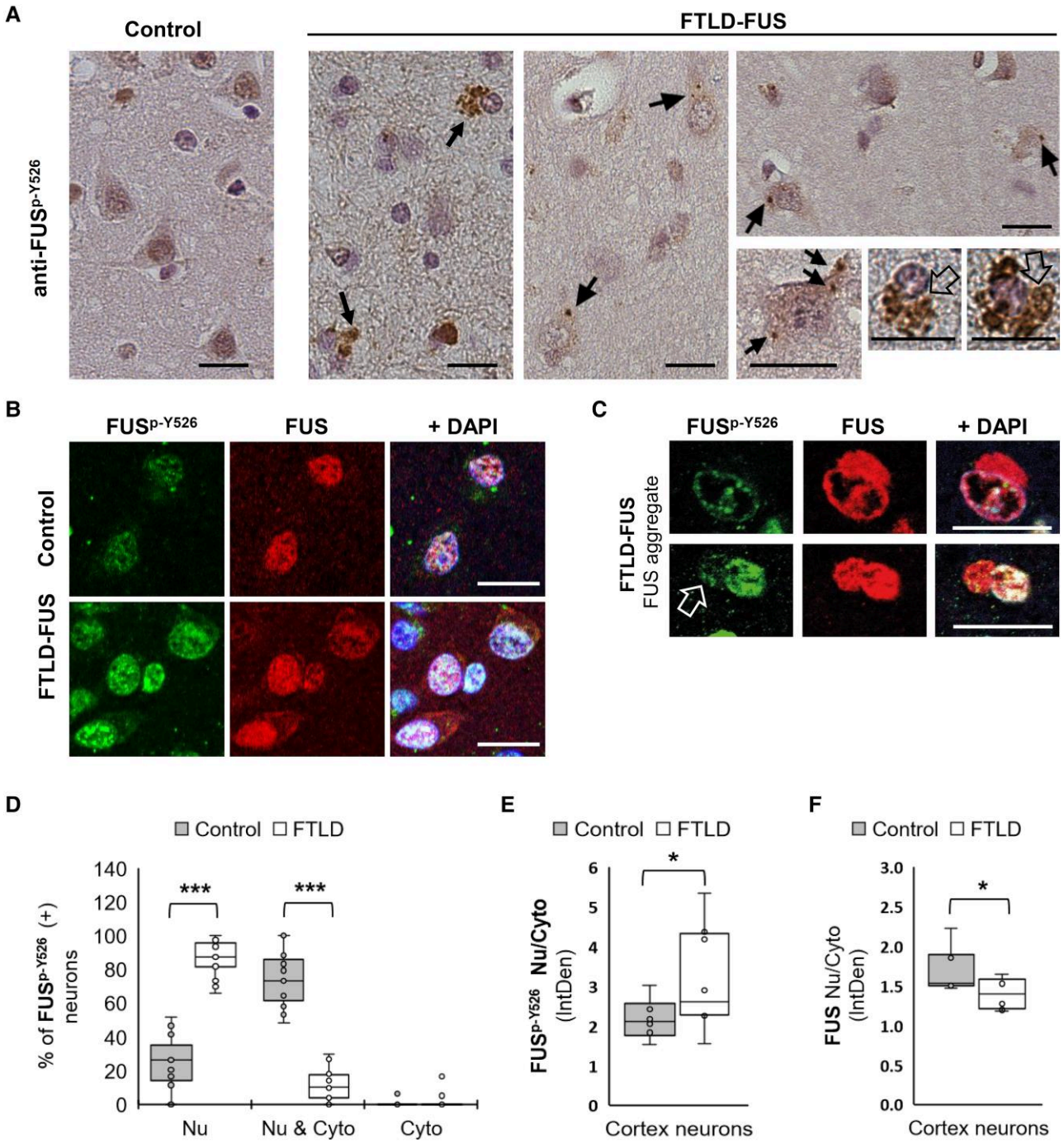

Figure 6 FUS$^{p\text{-}Y526}$ shows altered nucleocytoplasmic localization in cortical neurons in FTLD-FUS patients. (**A**) DAB immunolabelling using FUS$^{p\text{-}Y526}$ antibody in a representative control section showing diffuse nuclear immunoreactivity, whereas in FTLD-FUS cortical neurons (*right*) showing diffuse nuclear as well as cytoplasmic localization. FUS$^{p\text{-}Y526}$ antibody also recognizes smaller atypical granular (black arrows) and small globular (white arrow) aggregates. (**B**) Co-immunolabelling of FUS$^{p\text{-}Y526}$ and FUS in the cortical neurons of the control and FTLD-FUS patients, (**C**) showing the FUS and FUS$^{p\text{-}Y526\ signals}$ to only partially overlap in large cytoplasmic inclusions (white arrow). (**D**) Quantification of localization of the fluorescent FUS$^{p\text{-}Y526}$ immunolabelling (Nu = nuclear; Nu & Cyto = nuclear and cytoplasmic; Cyto = cytoplasmic only) by counting neurons in the frontal cortex of control and FTLD-FUS post-mortem brain tissue sections. ImageJ analyses of (**E**) FUS$^{p\text{-}Y526}$ and (**F**) FUS nuclear/cytoplasmic ratio in counted neurons. Statistical analyses were performed using ANOVA. Control $n = 4$, FTLD-FUS = 4. *$P < 0.05$, **$P < 0.01$. Paraffin sections, scale bar = 18 μm.

speculated to form higher-order complexes in rat brain lysates,[26] cells,[13,33] brains of transgenic FUS mice,[15] and in ALS-TDP43 patients.[50] The FUS$^{p\text{-}Y526}$ signal shift (to 130 kDa) in cAbl-expressing cells, could also be attributed to the processive c-Abl phosphorylation mode which is distinct from the distributive c-Src/c-Fyn phosphorylation mode[48] and is known to result in higher molecular weight signals of other hyperphosphorylated proteins.[49]

Second, we found that the intracellular localization and solubility (aggregation) of FUS$^{p\text{-}Y526}$ also depend on the kinase-type. Both c-Src and c-Fyn exhibited nuclear localization, whereas c-Abl

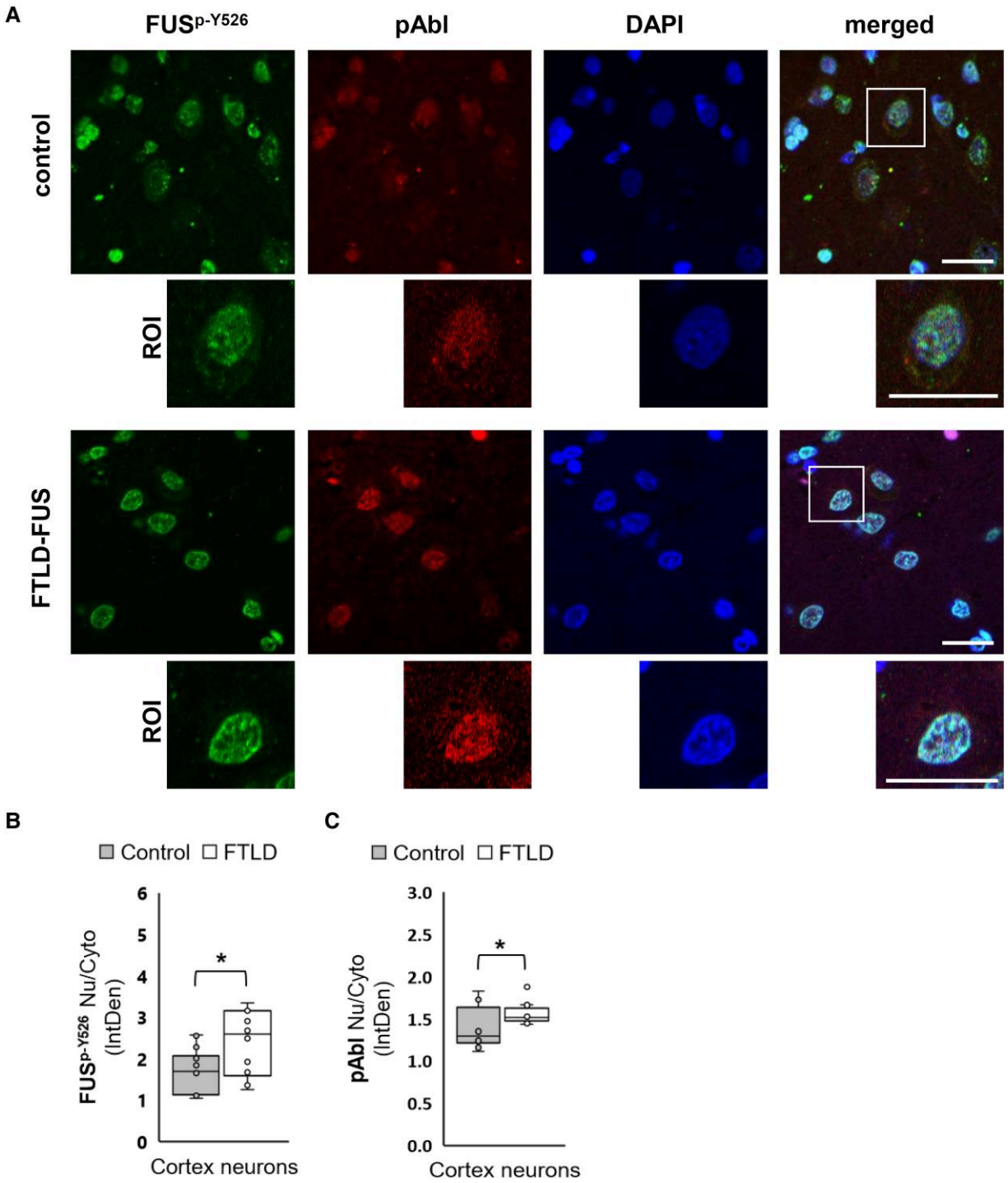

Figure 7 Activity of pAbl increases in the nuclei of FTLD-FUS frontal cortex neurons. (**A**) Co-immunolabelling using FUS$^{p\text{-}Y526}$ and pAbl antibody in the cortical neurons of control and FTLD-FUS patients. (**B**) Counting the frontal cortex neurons with pAbl signal localization in nucleus only (Nu), nucleus and cytoplasm (Nu & Cyto), or in the cytoplasm only (Cyto) in post-mortem tissue sections of control and FTLD-FUS. ImageJ analyses of (**C**) FUS$^{p\text{-}Y526}$ and (**D**) pAbl nuclear/cytoplasmic ratio in counted cortical neurons. Statistical analyses were performed using ANOVA. *$P < 0.05$, **$P < 0.01$. Paraffin sections, scale bar = 20 μm.

showed cytoplasmic activity, consistently overlapping with detected FUS$^{p\text{-}Y526}$ signal in kinase transfected cells (Fig. 3). Since kinase activity of c-Abl (preserved in Bcr-Abl fusion) has been shown to prevent proteasome-mediated proteolysis of FUS,[33,52] which in turn increases endogenous levels of FUS,[52] this could explain the increased FUS inclusions observed in cAbl expressing HEK293T cells. Additionally, c-Abl hyperphosphorylation of FUS, including Tyr526 of FUS, which inhibits FUS binding to TNPO1,[26] otherwise responsible for FUS solubility,[31] could also explain why cAbl phosphorylated FUS$^{p\text{-}Y526}$ was observed only in the insoluble fraction. Though this higher molecular weight signal of FUS has been reported by others,[13,15,26,33,50] we are the first to associate it with the c-Abl activity. Such hyperphosphorylated FUS may present changed epitopes and may not be detectable by antibodies

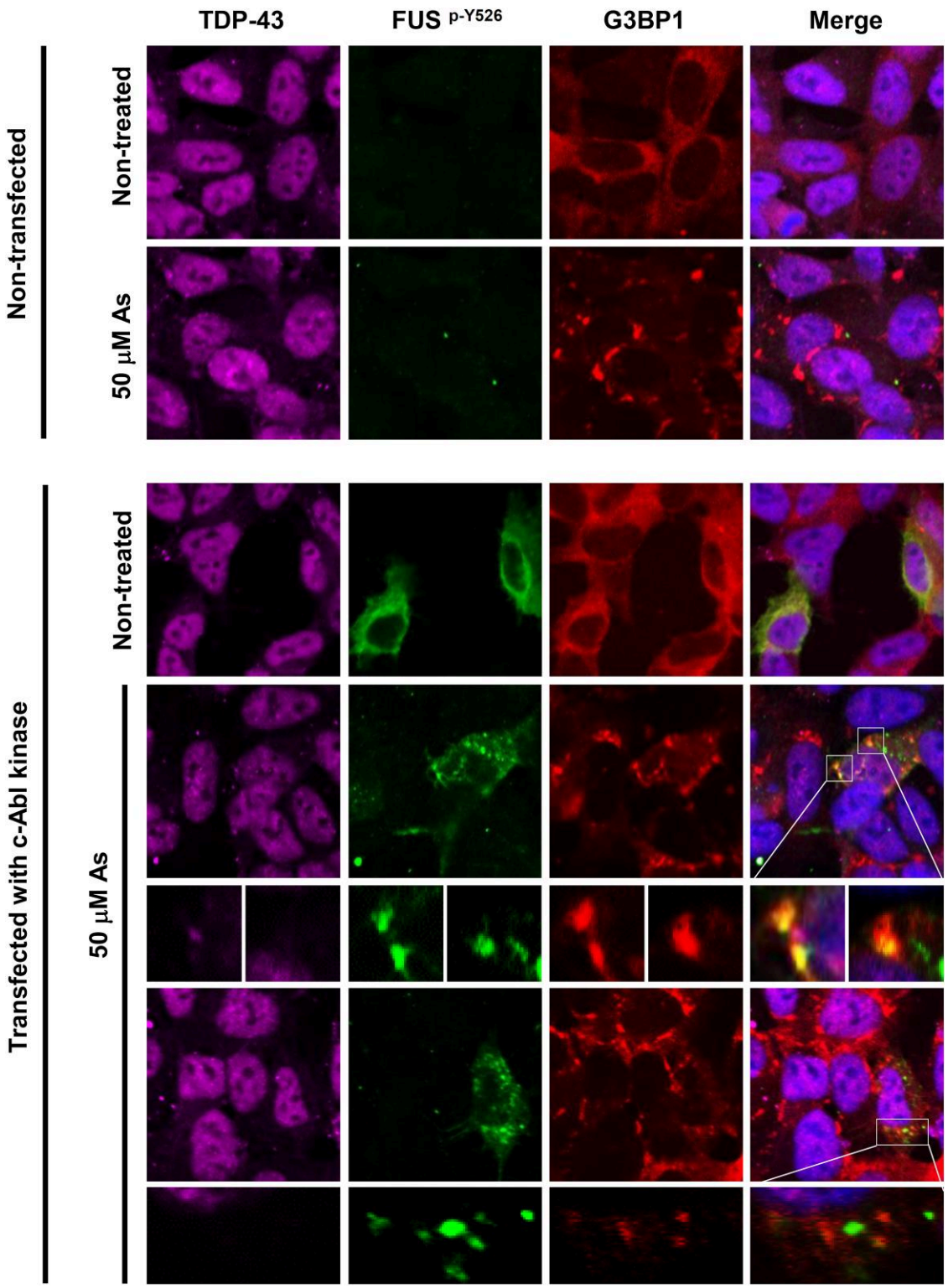

Figure 8 Activity of pAbl induces FUS$^{p\text{-}Y526}$ sequestration into G3BP1 positive granules in stressed sh-SY5Y. The FlpIn SH-SY5Y-TR-FRT-mScarlet-G3BP1-Myc cells generated by us were induced by doxycycline and transfected with constitutively active c-Abl kinase. Twenty hours post-transfection they were exposed to 50 μM sodium arsenite (As) for 1.5 h and processed for FUS$^{p\text{-}Y526}$ (green) and TDP-43 (magenta) immunolabelling, which revealed co-localization of FUS$^{p\text{-}Y526}$ and mScarlet-G3BP1 granules (red) only in stressed c-Abl transfected cells. The cell nuclei were counterstained with DAPI. Scale bar = 20 μm.

raised against unmodified FUS. It is worth noting that the majority of published data on FUS phosphorylation focuses on Ser/Thr phosphorylation of FUS LCD (N-terminal domain),[13,29,33] which decreases FUS aggregation.[29] However, our results suggest that cAbl-mediated FUS$^{p\text{-}Y526}$ phosphorylation increases cytoplasmic localization and aggregation propensity of FUS under stress conditions.

Our hypothesis was that C-terminal phosphorylation of FUS might be abundant in the brain, as increased c-Src/c-Abl kinase activity has also been demonstrated in Alzheimer's disease, Niemann-Pick type 2 disease, sporadic Parkinson's disease,[39] and proposed to coincide with the reduction in FUS turnover induced by c-Abl.[52] To confirm the presence of FUS$^{p\text{-}Y526}$ in more relevant tissues, we first analysed Tyr526 FUS phosphorylation in mouse brains, as Deng and colleagues had previously found that phosphorylated FUS LCD is present as a transient intermediate in the mouse brain.[33] Indeed, we detected FUS$^{p\text{-}Y526}$ positive neurons of mouse cortex, hippocampus and cerebellum. Overlapping patter of expression of pSrc and pFyn with FUS$^{p\text{-}Y526}$ signal was observed in neurons of the hippocampus that is consistent with the proposed role of FUS in this area,[60] whereas co-localization of FUS$^{p\text{-}Y526}$ signals and pAbl observed in neurons of the mouse cerebral cortex suggest the possible role of FUS$^{p\text{-}Y526}$ in human FUSopathies mainly affecting the frontal cortex, such as FTLD-FUS.

Immunoreactive patterns of FUS$^{p\text{-}Y526}$ antibody (against phosphor-Tyr526 of FUS) and pAbl in the frontal cortex of FTLD-FUS patients revealed a persistent nuclear localization of phosphorylated FUS$^{p\text{-}Y526}$ (Fig. 6). Such a phenomenon could be pathologically relevant for the majority of FTLD cases because of a strong nuclear retention of FUS$^{p\text{-}Y526}$. Although we could not detect significant co-localization of FUS$^{p\text{-}Y526}$ together with the typical compact FUS aggregates using routine commercial FUS antibodies, FUS$^{p\text{-}Y526}$ often appeared as atypical granular cytoplasmic aggregates, which were rarely co-localized with typical FUS aggregates. These finding raises the possibility that FUS$^{p\text{-}Y526}$ could be involved only in certain phases of FUS aggregation. In addition, such rare co-localization could suggest a novel role of FUS$^{p\text{-}Y526}$ to regulate early events in FUS aggregate formation. However, further experimental evidence is warranted to verify this notion. We also observed that pAbl showed a granular pattern of immunoreactivity in the cortical neurons and co-localized with FUS$^{p\text{-}Y526}$ (Fig. 7A), and the ratio of nuclear/cytoplasmic signal intensity indicated increased nuclear pAbl detection (Fig. 7B). Of note, c-Abl isomers *in vivo* can localize both to the nucleus as well as to the cytoplasm, and in neurodegenerative conditions, c-Abl isomers can be abnormally activated along with c-Src kinases.[32,36,37,39] Thus, it is reasonable to assume that such activation and differential localization of active pAbl may promote preferential FUS$^{p\text{-}Y526}$ retention in the nucleus of majority of cortical neurons in FTD-FUS. Similarly, our results also suggest that cytoplasmic pAbl-mediated phosphorylation of Tyr526 FUS might trigger the process of early cytoplasmic FUS aggregates and stress granules assembly, presumably under stress conditions (Fig. 8), because phospho-Tyr526 inhibits TNPO1 binding to FUS,[26] making entangled soluble FUS unavailable for TNPO1 unwinding,[31] possibly raising the local FUS concentration that upon de phosphorylation may allow for insoluble FUS aggregates formation (negative for FUS$^{p\text{-}Y526}$). Here it is particularly important to note that nucleocytoplasmic shuttling of FUS is not solely mediated by TNPO1 but can also be mediated by other import receptors to some extent.[61] We also observed more frequent FUS$^{p\text{-}Y526}$ staining in neurons and surrounding glia in human frontal cortex, as oppose to mice, which is likely due to the different activity of kinases observed in human and mouse neuronal cell models.[62] It will be interesting in the future to fully characterize these small globular and granular FUS$^{p\text{-}Y526}$ accumulations together with the interacting kinases to understand their pathophysiological role in FTLD-FUS. In summary, our study suggests that tyrosine kinase-driven post-translational modifications of FUS may be the upstream trigger of various pathophysiological changes leading to the development and progression of FTLD-FUS. Our generated antibody specifically recognizing FUS$^{p\text{-}Y526}$ revealed pAbl-mediated phosphorylation of Tyr526 FUS, which is critical for early pathophysiological events in FTLD-FUS and has not been previously recognized by commercial antibodies.

Acknowledgements

We thank Tomaž Marš for providing the anti-SMI33 and anti-A2B5 antibodies, Boris Turk, Janja Završnik, and Miha Butinar for the access to the mouse facility and help with the wild-type mice maintenance, Haihong Guo and Sven Kuspiel form Institute of Neuropathology and Institute of Physiology, RWTH Aachen University for providing primary cortical neurons and help with the staining and Vera Župunski from Faculty of Chemistry and Chemical Technology, University of Ljubljana, Slovenia, for help with biochemistry work. We acknowledge J. Anink (Amsterdam UMC location University of Amsterdam, Department of Neuropathology) for providing technical support.

Funding

This work was supported by the Slovenian Research Agency (grant numbers N3-0141, J3-9263, J3-8201, J3-3065, and P4-0127). E.A. was supported by the ALS Stichting (grant 'The Dutch ALS Tissue Bank').

Competing interests

The authors report no competing interests.

Supplementary material

Supplementary material is available at *Brain* online.

References

1. Kwiatkowski TJJ, Bosco DA, Leclerc AL, *et al*. Mutations in the FUS/TLS gene on chromosome 16 cause familial amyotrophic lateral sclerosis. *Science*. 2009;323:1205-1208.
2. Vance C, Rogelj B, Hortobágyi T, *et al*. Mutations in FUS, an RNA processing protein, cause familial amyotrophic lateral sclerosis type 6. *Science*. 2009;323:1208-1211.
3. Cairns NJ, Ghoshal N. FUS: a new actor on the frontotemporal lobar degeneration stage. *Neurology*. 2010;74:354-356.
4. Prpar Mihevc S, Darovic S, Kovanda A, Bajc Česnik A, Župunski V, Rogelj B. Nuclear trafficking in amyotrophic lateral sclerosis and frontotemporal lobar degeneration. *Brain*. 2017;140:13-26.
5. Sreedharan J, Blair IP, Tripathi VB, *et al*. TDP-43 mutations in familial and sporadic amyotrophic lateral sclerosis. *Science*. 2008; 319:1668-1672.
6. Tollervey JR, Curk T, Rogelj B, *et al*. Characterizing the RNA targets and position-dependent splicing regulation by TDP-43. *Nat Neurosci*. 2011;14:452-458.
7. Rogelj B, Easton LE, Bogu GK, *et al*. Widespread binding of FUS along nascent RNA regulates alternative splicing in the brain. *Sci Rep*. 2012;2:603.
8. Snowden JS, Hu Q, Rollinson S, *et al*. The most common type of FTLD-FUS (aFTLD-U) is associated with a distinct clinical form of frontotemporal dementia but is not related to mutations in the FUS gene. *Acta Neuropathol*. 2011;122:99-110.

9. Rhine K, Makurath MA, Liu J, *et al*. ALS/FTLD-Linked mutations in FUS glycine residues cause accelerated gelation and reduced interactions with wild-type FUS. *Mol Cell*. 2020;80:666-681.e8.
10. Naumann M, Laubenthal J, Hermann A. Fused in sarcoma-amyotrophic lateral sclerosis as a novel member of DNA single strand break diseases with pure neurological phenotypes. *Neural Regen Res*. 2021;16:110-112.
11. Troakes C, Hortobágyi T, Vance C, Al-Sarraj S, Rogelj B, Shaw CE. Transportin 1 colocalization with fused in sarcoma (FUS) inclusions is not characteristic for amyotrophic lateral sclerosis-FUS confirming disrupted nuclear import of mutant FUS and distinguishing it from frontotemporal lobar degeneration with FUS inclusions. *Neuropathol Appl Neurobiol*. 2013;39:553-561.
12. Ding X, Sun F, Chen J, *et al*. Amyloid-Forming segment induces aggregation of FUS-LC domain from phase separation modulated by site-specific phosphorylation. *J Mol Biol*. 2020;432:467-483.
13. Rhoads SN, Monahan ZT, Yee DS, *et al*. The prionlike domain of FUS is multiphosphorylated following DNA damage without altering nuclear localization. *Mol Biol Cell*. 2018;29:1786-1797.
14. López-Erauskin J, Tadokoro T, Baughn MW, *et al*. ALS/FTD-linked mutation in FUS suppresses intra-axonal protein synthesis and drives disease without nuclear loss-of-function of FUS. *Neuron*. 2018;100:816-830.e7.
15. Lysikova EA, Kukharsky MS, Chaprov KD, *et al*. Behavioural impairments in mice of a novel FUS transgenic line recapitulate features of frontotemporal lobar degeneration. *Genes Brain Behav*. 2019;18:e12607.
16. Lysikova EA, Funikov S, Rezvykh AP, *et al*. Low level of expression of C-terminally truncated human FUS causes extensive changes in the spinal cord transcriptome of asymptomatic transgenic mice. *Neurochem Res*. 2020;45:1168-1179.
17. Shelkovnikova TA, Peters OM, Deykin AV, *et al*. Fused in sarcoma (FUS) protein lacking nuclear localization signal (NLS) and major RNA binding motifs triggers proteinopathy and severe motor phenotype in transgenic mice. *J Biol Chem*. 2013;288:25266-25274.
18. Mitchell JC, McGoldrick P, Vance C, *et al*. Overexpression of human wild-type FUS causes progressive motor neuron degeneration in an age- and dose-dependent fashion. *Acta Neuropathol*. 2013;125:273-288.
19. Kang J, Lim L, Song J. ATP Enhances at low concentrations but dissolves at high concentrations liquid-liquid phase separation (LLPS) of ALS/FTD-causing FUS. *Biochem Biophys Res Commun*. 2018;504:545-551.
20. Murray DT, Kato M, Lin Y, *et al*. Structure of FUS protein fibrils and its relevance to self-assembly and phase separation of low-complexity domains. *Cell*. 2017;171:615-627.e16.
21. Shorter J. Liquidizing FUS via prion-like domain phosphorylation. *EMBO J*. 2017;36:2925-2927.
22. Ikenaka K, Ishigaki S, Iguchi Y, *et al*. Characteristic features of FUS inclusions in spinal motor neurons of sporadic amyotrophic lateral sclerosis. *J Neuropathol Exp Neurol*. 2020;79:370-377.
23. Tischbein M, Baron DM, Lin Y-C, *et al*. The RNA-binding protein FUS/TLS undergoes calcium-mediated nuclear egress during excitotoxic stress and is required for GRIA2 mRNA processing. *J Biol Chem*. 2019;294:10194-10210.
24. Lindström M, Liu B. Yeast as a model to unravel mechanisms behind FUS toxicity in amyotrophic lateral sclerosis. *Front Mol Neurosci*. 2018;11:218.
25. Owen I, Shewmaker F. The role of post-translational modifications in the phase transitions of intrinsically disordered proteins. *Int J Mol Sci*. 2019;20:5501.
26. Darovic S, Prpar Mihevc S, Župunski V, *et al*. Phosphorylation of C-terminal tyrosine residue 526 in FUS impairs its nuclear import. *J Cell Sci*. 2015;128:4151-4159.
27. Qamar S, Wang G, Randle SJ, *et al*. FUS Phase separation is modulated by a molecular chaperone and methylation of arginine cation-π interactions. *Cell*. 2018;173:720-734.e15.
28. Hofweber M, Hutten S, Bourgeois B, *et al*. Phase separation of FUS is suppressed by its nuclear import receptor and arginine methylation. *Cell*. 2018;173:706-719.e13.
29. Monahan Z, Ryan VH, Janke AM, *et al*. Phosphorylation of the FUS low-complexity domain disrupts phase separation, aggregation, and toxicity. *EMBO J*. 2017;36:2951-2967.
30. Yoshizawa T, Ali R, Jiou J, *et al*. Nuclear import receptor inhibits phase separation of FUS through binding to multiple sites. *Cell*. 2018;173:693-705.e22.
31. Guo L, Kim HJ, Wang H, *et al*. Nuclear-Import receptors reverse aberrant phase transitions of RNA-binding proteins with prion-like domains. *Cell*. 2018;173:677-692.e20.
32. Palomo V, Nozal V, Rojas-Prats E, Gil C, Martinez A. Protein kinase inhibitors for amyotrophic lateral sclerosis therapy. *Br J Pharmacol*. 2021;178:1316-1335.
33. Deng Q, Holler CJ, Taylor G, *et al*. FUS Is phosphorylated by DNA-PK and accumulates in the cytoplasm after DNA damage. *J Neurosci*. 2014;34:7802-7813.
34. Owen I, Rhoads S, Yee D, *et al*. The prion-like domain of fused in sarcoma is phosphorylated by multiple kinases affecting liquid- and solid-phase transitions. *Mol Biol Cell*. 2020;31:2522-2536.
35. Ait-Bouziad N, Chiki A, Limorenko G, Xiao S, Eliezer D, Lashuel HA. Phosphorylation of the overlooked tyrosine 310 regulates the structure, aggregation, and microtubule- and lipid-binding properties of tau. *J Biol Chem*. 2020;295:7905-7922.
36. Kim BW, Jeong YE, Wong M, Martin LJ. DNA Damage accumulates and responses are engaged in human ALS brain and spinal motor neurons and DNA repair is activatable in iPSC-derived motor neurons with SOD1 mutations. *Acta Neuropathol Commun*. 2020;8:7.
37. Lim SL, Tran DN, Kieu Z, *et al*. Genetic ablation of hematopoietic cell kinase accelerates Alzheimer's disease-like neuropathology in Tg2576 mice. *Mol Neurobiol*. 2020;57:2447-2460.
38. Gutierrez DA, Vargas LM, Chandia-Cristi A, de la Fuente C, Leal N, Alvarez AR. c-Abl deficiency provides synaptic resiliency against Aβ-oligomers. *Front Cell Neurosci*. 2019;13:526.
39. Ko HS, Lee Y, Shin J-H, *et al*. Phosphorylation by the c-abl protein tyrosine kinase inhibits parkin's ubiquitination and protective function. *Proc Natl Acad Sci U S A*. 2010;107:16691-16696.
40. Cheong HSJ, Nona M, Guerra SB, VanBerkum MF. The first quarter of the C-terminal domain of abelson regulates the WAVE regulatory complex and enabled in axon guidance. *Neural Dev*. 2020;15:7.
41. Nagaraj V, Theis T, Johal AS, *et al*. Application of antibodies to neuronally expressed Nogo-A increases neuronal survival and neurite outgrowth. *Int J Mol Sci*. 2020;21:5417.
42. Luttrell LM, Ferguson SS, Daaka Y, *et al*. Beta-arrestin-dependent formation of beta2 adrenergic receptor-src protein kinase complexes. *Science*. 1999;283:655-661.
43. Motaln H, Čerček U, Recek N, Bajc Česnik A, Mozetič M, Rogelj B. Cold atmospheric plasma induces stress granule formation via an eIF2α-dependent pathway. *Biomater Sci*. 2020;8:5293-5305.
44. Božič J, Motaln H, Janež AP, *et al*. Interactome screening of C9orf72 dipeptide repeats reveals VCP sequestration and functional impairment by polyGA. *Brain*. 2022;145:684-699.
45. Nango H, Kosuge Y, Sato M, *et al*. Highly efficient conversion of motor neuron-like NSC-34 cells into functional motor neurons by prostaglandin E(2). *Cells*. 2020;9:1741.
46. Tripathi P, Guo H, Dreser A, *et al*. Pathomechanisms of ALS8: altered autophagy and defective RNA binding protein (RBP) homeostasis due to the VAPB P56S mutation. *Cell Death Dis*. 2021;12:466.
47. Yamoah A, Tripathi P, Sechi A, *et al*. Aggregates of RNA binding proteins and ER chaperones linked to exosomes in

granulovacuolar degeneration of the Alzheimer's disease brain. *J Alzheimers Dis*. 2020;75:139-156.
48. Dephoure N, Gould KL, Gygi SP, Kellogg DR. Mapping and analysis of phosphorylation sites: a quick guide for cell biologists. *Mol Biol Cell*. 2013;24:535-542.
49. Duyster J, Baskaran R, Wang JY. Src homology 2 domain as a specificity determinant in the c-abl-mediated tyrosine phosphorylation of the RNA polymerase II carboxyl-terminal repeated domain. *Proc Natl Acad Sci U S A*. 1995;92:1555-1559.
50. Hernandez Lain A, Millecamps S, Dubourg O, *et al*. Abnormal TDP-43 and FUS proteins in muscles of sporadic IBM: similarities in a TARDBP-linked ALS patient. *J Neurol Neurosurg Psychiatry*. 2011;82:1414-1416.
51. Imamura K, Izumi Y, Watanabe A, *et al*. The src/c-abl pathway is a potential therapeutic target in amyotrophic lateral sclerosis. *Sci Transl Med*. 2017;9:eaaf3962.
52. Perrotti D, Iervolino A, Cesi V, *et al*. BCR-ABL prevents c-jun-mediated and proteasome-dependent FUS (TLS) proteolysis through a protein kinase CbetaII-dependent pathway. *Mol Cell Biol*. 2000;20:6159-6169.
53. Vance C, Scotter EL, Nishimura AL, *et al*. ALS Mutant FUS disrupts nuclear localization and sequesters wild-type FUS within cytoplasmic stress granules. *Hum Mol Genet*. 2013;22:2676-2688.
54. Chen C, Ding X, Akram N, Xue S, Luo S-Z. Fused in sarcoma: properties, self-assembly and correlation with neurodegenerative diseases. *Molecules*. 2019;24:1622.
55. Dormann D, Rodde R, Edbauer D, *et al*. ALS-associated fused in sarcoma (FUS) mutations disrupt transportin-mediated nuclear import. *EMBO J*. 2010;29:2841-2857.
56. Scekic-Zahirovic J, Sendscheid O, El Oussini H, *et al*. Toxic gain of function from mutant FUS protein is crucial to trigger cell autonomous motor neuron loss. *EMBO J*. 2016;35:1077-1097.
57. Neumann M, Valori CF, Ansorge O, *et al*. Transportin 1 accumulates specifically with FET proteins but no other transportin cargos in FTLD-FUS and is absent in FUS inclusions in ALS with FUS mutations. *Acta Neuropathol*. 2012;124:705-716.
58. Suárez-Calvet M, Neumann M, Arzberger T, *et al*. Monomethylated and unmethylated FUS exhibit increased binding to transportin and distinguish FTLD-FUS from ALS-FUS. *Acta Neuropathol*. 2016;131:587-604.
59. Gschwendt M, Kielbassa K, Kittstein W, Marks F. Tyrosine phosphorylation and stimulation of protein kinase C delta from porcine spleen by src in vitro. Dependence on the activated state of protein kinase C delta. *FEBS Lett*. 1994;347:85-89.
60. Kino Y, Washizu C, Kurosawa M, *et al*. FUS/TLS deficiency causes behavioral and pathological abnormalities distinct from amyotrophic lateral sclerosis. *Acta Neuropathol Commun*. 2015;3:24.
61. Baade I, Hutten S, Sternburg EL, *et al*. The RNA-binding protein FUS is chaperoned and imported into the nucleus by a network of import receptors. *J Biol Chem*. 2021;296:100659.
62. Johnson MA, Deng Q, Taylor G, *et al*. Divergent FUS phosphorylation in primate and mouse cells following double-strand DNA damage. *Neurobiol Dis*. 2020;146:105085.